Biomedical Optics EXPRESS

Effect of recombinant interleukin-12 on murine skin regeneration and cell dynamics using *in vivo* multimodal microscopy

Joanne Li,[1,4] Andrew J. Bower,[2,4] Vladimir Vainstein,[5] Zoya Gluzman-Poltorak,[5] Eric J. Chaney,[4] Marina Marjanovic,[1,4] Lena A. Basile,[5] and Stephen A. Boppart[1,2,3,4,*]

[1]*Department of Bioengineering, University of Illinois at Urbana-Champaign, 1270 Digital Computer Laboratory, MC-278, 1304 W. Springfield Ave. Urbana, IL 61801, USA*
[2]*Department of Electrical and Computer Engineering, University of Illinois at Urbana-Champaign, 306 N. Wright St. Urbana, IL 61801, USA*
[3]*Department of Internal Medicine, University of Illinois at Urbana-Champaign, 190 Medical Science Building, MC-714, 506 S. Mathews Ave. Urbana, IL 61801, USA*
[4]*Beckman Institute for Advanced Science and Technology, University of Illinois at Urbana-Champaign, 405 N. Mathews Ave. Urbana, IL 61801, USA*
[5]*Neumedicines Inc. 133 N. Altadena Dr. #310, Pasadena, CA 91107, USA*
**boppart@illinois.edu*

Abstract: Interleukin-12 (IL-12) is a pro-inflammatory cytokine known for its role in immunity, and previous studies have shown that IL-12 provides mitigation of radiation injury. In this study, we utilize a multimodal microscopy system equipped with second harmonic generation (SHG) and fluorescence lifetime imaging microscopy (FLIM) to examine the effect of IL-12 on collagen structure and cellular metabolic activity *in vivo* during skin wound healing. This preliminary study illustrates the highly dynamic and heterogeneous *in vivo* microenvironment of the wounded skin. In addition, results suggest that IL-12 triggers a significantly more rapid and greater cellular metabolic response in the wounded animals. These results can elucidate insights into the response mechanism of IL-12 in both wound healing and acute radiation syndrome.

OCIS codes: (180.4315) Nonlinear microscopy; (170.2520) Fluorescence microscopy; (170.6920) Time-resolved imaging; (190.1900) Diagnostic applications of nonlinear optics; (170.3880) Medical and biological imaging

References and links

1. G. Trinchieri, "Interleukin-12 and the regulation of innate resistance and adaptive immunity," Nat. Rev. Immunol. **3**(2), 133–146 (2003).
2. S. A. Gerber, R. J. Cummings, J. L. Judge, M. L. Barlow, J. Nanduri, D. E. Johnson, J. Palis, A. P. Pentland, E. M. Lord, and J. L. Ryan, "Interleukin-12 preserves the cutaneous physical and immunological barrier after radiation exposure," Radiat. Res. **183**(1), 72–81 (2015).
3. M. B. Witte and A. Barbul, "General principles of wound healing," Surg. Clin. North Am. **77**(3), 509–528 (1997).
4. Z. Gluzman-Poltorak, V. Vainstein, and L. A. Basile, "Recombinant interleukin-12, but not granulocyte-colony stimulating factor, improves survival in lethally irradiated nonhuman primates in the absence of supportive care: evidence for the development of a frontline radiation medical countermeasure," Am. J. Hematol. **89**(9), 868–873 (2014).
5. F. H. Epstein, A. J. Singer, and R. A. F. Clark, "Cutaneous wound healing," N. Engl. J. Med. **341**(10), 738–746 (1999).
6. P. Martin, "Wound healing--aiming for perfect skin regeneration," Science **276**(5309), 75–81 (1997).
7. J. Li, J. Chen, and R. Kirsner, "Pathophysiology of acute wound healing," Clin. Dermatol. **25**(1), 9–18 (2007).
8. B. W. Graf, E. J. Chaney, M. Marjanovic, S. G. Adie, M. De Lisio, M. C. Valero, M. D. Boppart, and S. A. Boppart, "Long-term time-lapse multimodal intravital imaging of regeneration and bone-marrow-derived cell dynamics in skin," Technology **1**(1), 8–19 (2013).

#243477 Received 22 Jun 2015; revised 20 Sep 2015; accepted 29 Sep 2015; published 6 Oct 2015

9. M. C. Skala, K. M. Riching, A. Gendron-Fitzpatrick, J. Eickhoff, K. W. Eliceiri, J. G. White, and N. Ramanujam, "*In vivo* multiphoton microscopy of NADH and FAD redox states, fluorescence lifetimes, and cellular morphology in precancerous epithelia," Proc. Natl. Acad. Sci. U.S.A. **104**(49), 19494–19499 (2007).
10. A. J. Walsh and M. C. Skala, "Optical metabolic imaging quantifies heterogeneous cell populations," Biomed. Opt. Express **6**(2), 559–573 (2015).
11. M. Balu, K. M. Kelly, C. B. Zachary, R. M. Harris, T. B. Krasieva, K. König, A. J. Durkin, and B. J. Tromberg, "Distinguishing between benign and malignant melanocytic nevi by *in vivo* multiphoton microscopy," Cancer Res. **74**(10), 2688–2697 (2014).
12. P. J. Campagnola and L. M. Loew, "Second-harmonic imaging microscopy for visualizing biomolecular arrays in cells, tissues and organisms," Nat. Biotechnol. **21**(11), 1356–1360 (2003).
13. J. R. Lakowicz, H. Szmacinski, K. Nowaczyk, and M. L. Johnson, "Fluorescence lifetime imaging of free and protein-bound NADH," Proc. Natl. Acad. Sci. U.S.A. **89**(4), 1271–1275 (1992).
14. B. W. Graf, A. J. Bower, E. J. Chaney, M. Marjanovic, S. G. Adie, M. De Lisio, M. C. Valero, M. D. Boppart, and S. A. Boppart, "*In vivo* multimodal microscopy for detecting bone-marrow-derived cell contribution to skin regeneration," J. Biophotonics **7**(1-2), 96–102 (2014).
15. S. Wu, H. Li, H. Yang, X. Zhang, Z. Li, and S. Xu, "Quantitative analysis on collagen morphology in aging skin based on multiphoton microscopy," J. Biomed. Opt. **16**(4), 040502 (2011).
16. R. A. Rao, M. R. Mehta, and K. C. Toussaint, Jr., "Fourier transform-second-harmonic generation imaging of biological tissues," Opt. Express **17**(17), 14534–14542 (2009).
17. P. D. Dale, J. A. Sherratt, and P. K. Maini, "A mathematical model for collagen fibre formation during foetal and adult dermal wound healing," Proc. Biol. Sci. **263**(1370), 653–660 (1996).
18. D. K. Bird, L. Yan, K. M. Vrotsos, K. W. Eliceiri, E. M. Vaughan, P. J. Keely, J. G. White, and N. Ramanujam, "Metabolic mapping of MCF10A human breast cells via multiphoton fluorescence lifetime imaging of the coenzyme NADH," Cancer Res. **65**(19), 8766–8773 (2005).
19. M. Balu, A. Mazhar, C. K. Hayakawa, R. Mittal, T. B. Krasieva, K. König, V. Venugopalan, and B. J. Tromberg, "*In vivo* multiphoton NADH fluorescence reveals depth-dependent keratinocyte metabolism in human skin," Biophys. J. **104**(1), 258–267 (2013).
20. M. S. Roberts, Y. Dancik, T. W. Prow, C. A. Thorling, L. L. Lin, J. E. Grice, T. A. Robertson, K. König, and W. Becker, "Non-invasive imaging of skin physiology and percutaneous penetration using fluorescence spectral and lifetime imaging with multiphoton and confocal microscopy," Eur. J. Pharm. Biopharm. **77**(3), 469–488 (2011).
21. R. Niesner, B. Peker, P. Schlüsche, and K. H. Gericke, "Noniterative biexponential fluorescence lifetime imaging in the investigation of cellular metabolism by means of NAD(P)H autofluorescence," ChemPhysChem **5**(8), 1141–1149 (2004).
22. M. J. Im and J. E. Hoopes, "Energy metabolism in healing skin wounds," J. Surg. Res. **10**(10), 459–464 (1970).
23. K. Blinova, S. Carroll, S. Bose, A. V. Smirnov, J. J. Harvey, J. R. Knutson, and R. S. Balaban, "Distribution of mitochondrial NADH fluorescence lifetimes: steady-state kinetics of matrix NADH interactions," Biochemistry **44**(7), 2585–2594 (2005).
24. A. Mayevsky, "Mitochondrial function and energy metabolism in cancer cells: past overview and future perspectives," Mitochondrion **9**(3), 165–179 (2009).
25. M. Saraste, "Oxidative phosphorylation at the fin de siècle," Science **283**(5407), 1488–1493 (1999).

1. Introduction

Interleukin-12 (IL-12) is a pro-inflammatory cytokine primarily produced by monocytes, macrophages, and dendritic cells that is known to be involved in the development of cell-mediated immunity, and to form a link between innate resistance and adaptive immunity [1, 2]. IL-12 induces the production of interferon-gamma (IFN-γ), which is a cytokine with antiviral activity and has an essential role in resistance to many foreign pathogens [1]. Once released, IFN-γ can interact with nearby cells through paracrine signaling to ensure the continuous presence of essential cytokines and immune cells [3]. Recent studies have found that administration of IL-12 post-irradiation significantly reduces the size of burn wounds caused by radiation exposure, and can also increase the survival rate in lethally irradiated nonhuman primates [2, 4]. To better understand the functions of IL-12 in actively healing skin, a technology capable of noninvasive *in vivo* monitoring of the wounded skin and the cellular activity at single-cell resolution is imperative.

Injury triggers a complex and organized cascade of cellular and biochemical events that eventually lead to healed skin. However, this healed skin is not as structurally and functionally strong as non-wounded skin [5, 6]. In general, there are three stages during the process of wound healing: inflammation, proliferation, and remodeling [3, 5, 6]. The inflammatory stage is an essential phase of healing, during which cytokines, growth factors, and immune cells including macrophage and dendritic cells are released and activated [1, 3].

#243477 Received 22 Jun 2015; revised 20 Sep 2015; accepted 29 Sep 2015; published 6 Oct 2015

During the proliferation stage, the main activities involve skin resurfacing where formation of epithelium occurs to cover the wound surface, and dermal restoration including angiogenesis to pervade the wound space [5, 7]. Once the new tissue is formed, the remodeling phase begins to restore tissue integrity and functional competence [7]. While studies have discovered that IL-12 significantly reduces the severity of burn wounds and related acute radiation syndrome, the mode of action of this cytokine in minimizing radiation-induced cutaneous damage is still relatively unknown [2]. By investigating the change in the microenvironment of wounded skin after the administration of IL-12, we may gain valuable insights into the underlying mechanisms of how IL-12 assists in the skin recovery after radiation damages.

Multiphoton microscopy, including second-harmonic generation (SHG) microscopy and fluorescence lifetime microscopy (FLIM), is uniquely suited to study the skin microenvironment *in vivo* due to the high resolution and label-free imaging capabilities [8–11]. SHG is a nonlinear optical technique that generates contrast from the noncentrosymmetric organization of molecules, and has been widely utilized to investigate collagen, a major constituent in the dermis of skin [12]. FLIM probes the excited state lifetime of endogenous and exogenous fluorophores [13]. In metabolic imaging, dynamic profiles of cellular metabolism can be obtained from the fluorescence properties of the coenzyme, reduced nicotinamide adenine dinucleotide (NADH), which is involved in metabolism [9, 10]. NADH has a short and long lifetime component depending on whether the enzyme is in a free or protein-bound state, respectively, and is involved in many metabolic processes including glycolysis and oxidative phosphorylation [9, 13]. Therefore, changes in the fluorescence lifetime can help to elucidate the metabolic activity in cells.

In this study, structural and metabolic changes of the skin treated with recombinant murine IL-12 (rMuIL-12) were evaluated *in vivo* using a multimodal microscopy system that was equipped with SHG and FLIM modalities. SHG was used to track and quantify the collagen reformation during wound healing, and FLIM was used to probe the effect of IL-12 on the cellular metabolic activity in the keratinocytes of the epidermal layers of the skin. The acquired information has the potential to provide additional insights regarding the role of IL-12 in wounded skin.

2. Materials and methods

2.1 Animals, skin preparation, and wounding

All animal procedures were performed under a protocol approved by the Institutional Animal Care and Use Committee (IACUC) at the University of Illinois at Urbana-Champaign. Female C57BL/6 wild-type mice were used in this study. Prior to wounding under anesthesia (1% isofluorane gas mixed with 1.5% oxygen), the hair on the lower dorsal skin was first shaved with electric clippers (Peanut palm size clipper 8652, Wahl). For the region to be wounded and imaged, the remaining hair was further removed carefully using surgical forceps under a surgical microscope. The shaved skin was then cleaned with 70% ethanol, and full thickness excisional wounds were made using a sterile 1 mm biopsy punch (Miltex, Inc.). The wounds were left uncovered, and no analgesics or additional anti-inflammatory agents were administered to the mice during the course of the study.

2.2 Study design and recombinant murine interleukin-12 (rMuIL-12) treatment

Both the rMuIL-12 and placebo compounds were provided by Neumedicines, Inc. The study included three experimental groups (n = 5 per group): non-wounded mice with rMuIL-12 injection, wounded mice with placebo injection, and wounded mice with rMuIL-12 injection. The non-wounded group was imaged using the microscope system on days 0, 1 (pre-drug injection), 2, 3, 7, and 14. The two wounded groups were imaged on days 0 (pre-wounding), 1 (pre-drug injection), 2, 3, 5, 7, 14, 21, and 28. Approximately 8 hours after wounding and

#243477 Received 22 Jun 2015; revised 20 Sep 2015; accepted 29 Sep 2015; published 6 Oct 2015

imaging on day 1, prepared rMuIL-12 (40 ng/mouse) or placebo were administered by a single subcutaneous injection on the nape of the neck using a syringe needle with a dose volume of 100 µL/mouse.

2.3 Multimodal microscope

The multimodal microscope was a custom-built integrated multiphoton microscope (MPM) system, shown in Fig. 1 [8, 14].

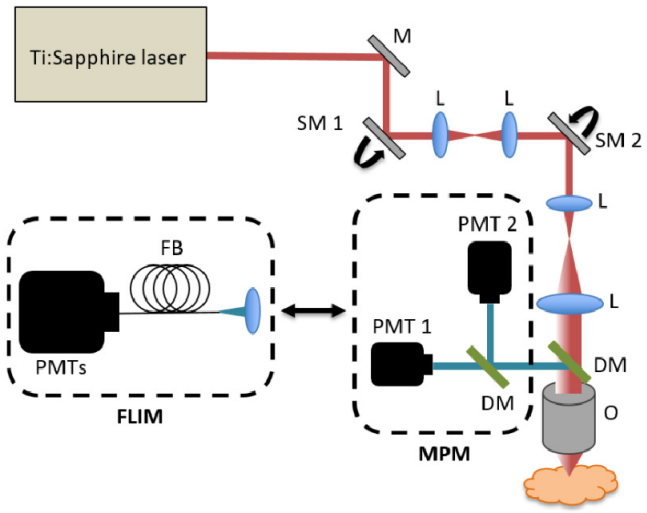

Fig. 1. Schematic of the multimodal microscope. Abbreviations: M – mirror, SM - scanning mirror, L - lens; DM -dichroic mirror, O - objective lens, PMT - photomultiplier tube, FB - fiber bundle.

The system utilized a laser source based on a tunable titanium:sapphire laser (Mai Tai HP, Spectra Physics). The center wavelength of the excitation was 920 nm for SHG imaging to eliminate unwanted background signals and 730 nm for FLIM imaging to achieve optimal excitation of NADH. The laser beam was directed through the sample arm and focused onto the sample using a 0.95 NA objective lens (XLUMP20X, Olympus). SHG signals were detected by a photomultiplier tube (PMT) through a 460 nm band-pass filter, and FLIM signals were measured by a 16-channel PMT spectrometer (PML-16-C, Becker-Hickl) through a 633 nm low-pass filter. To perform FLIM, the MPM PMTs were switched to the FLIM PMT without moving the rest of the sample arm components or the animals, as shown in Fig. 1.

2.4 Image acquisition and processing

SHG imaging of the skin around the wound was acquired with dimensions of approximately 2 x 2 mm^2 using a motorized stage to scan in the lateral dimensions. Images were acquired as 10 by 10 frame mosaics that were stitched together in post-processing using Matlab (Mathworks) and ImageJ (National Institutes of Health). In addition, volumetric SHG data with dimensions of 185 × 185 μm^2 across a depth of approximately 80 µm with 6-8 µm incremental steps were also acquired from around the wound. FLIM imaging was performed on four manually selected locations on the skin around the wound to sample the region. Time-correlated single photon counting (TCSPC) was performed using a commercial TCSPC data acquisition board (SPC-150, Becker-Hickl) to capture the fluorescence decay curves. The images were processed with SPCimage software (Becker-Hickl), and the average fluorescence lifetime of the entire image was calculated. The average and standard deviation

#243477 Received 22 Jun 2015; revised 20 Sep 2015; accepted 29 Sep 2015; published 6 Oct 2015

of the fluorescence lifetimes were evaluated, and one-way ANOVA combined with Tukey honest significant difference (HSD) test was used to determine the significance level.

2.5 Collagen alignment analysis

Collagen alignment analysis was performed on the SHG images of all animals. On each SHG image, five small areas with dimensions of approximately 150 x 150 pixels (108 × 108 μm^2) within 500 μm from the edge of the wounds were manually selected to avoid the dark signal-free regions in the hair follicles and the wounds. Also, these small image areas were manually selected because the change in collagen structure was more pronounced closer to the wound. Two-dimensional spatial Fourier transforms (FT) were performed on these small image blocks, and the FT magnitude images were converted into binary images based on a specified threshold. An ellipse-fit was then performed on these binary images utilizing the Matlab Image Processing Toolbox function and the parametric form of the ellipse equation [15]. To quantify the collagen structure around the wound bed, eccentricity of the ellipse was used, which was defined by Matlab as the ratio of the distance between the foci of the ellipse and its major axis length. The value was between 0 and 1. A value closer to 0 suggested that the collagen fibers in the selected regions were isotropically distributed, and a value closer to 1 suggested that the collagen fibers were more aligned in a particular direction. The average and standard deviation of the eccentricity values were calculated, and one-way ANOVA combined with Tukey HSD test was utilized to evaluate the significance level.

3. Results and discussion

3.1 Collagen structure and alignment

SHG was utilized to track the progress of wound healing and to evaluate the collagen structure around the wound bed within the first 100 μm depth of the dermal skin layer. Figure 2 illustrates the progress of wound healing during the one month period. SHG imaging showed that there appeared to have an active collagen contraction between days 5 and 14, which is a part of the remodeling stage of wound healing characterized by a more aligned collagen structure [7]. By days 21 and 28, the collagen structure on top of the wounds appeared to be mostly restored, but with a lower collagen fiber density compared to the surrounding non-wounded areas. The weaker SHG signals observed in the wound bed suggested that there was a lower type I collagen density since type I collagen gives stronger SHG signals [12].

#243477 Received 22 Jun 2015; revised 20 Sep 2015; accepted 29 Sep 2015; published 6 Oct 2015

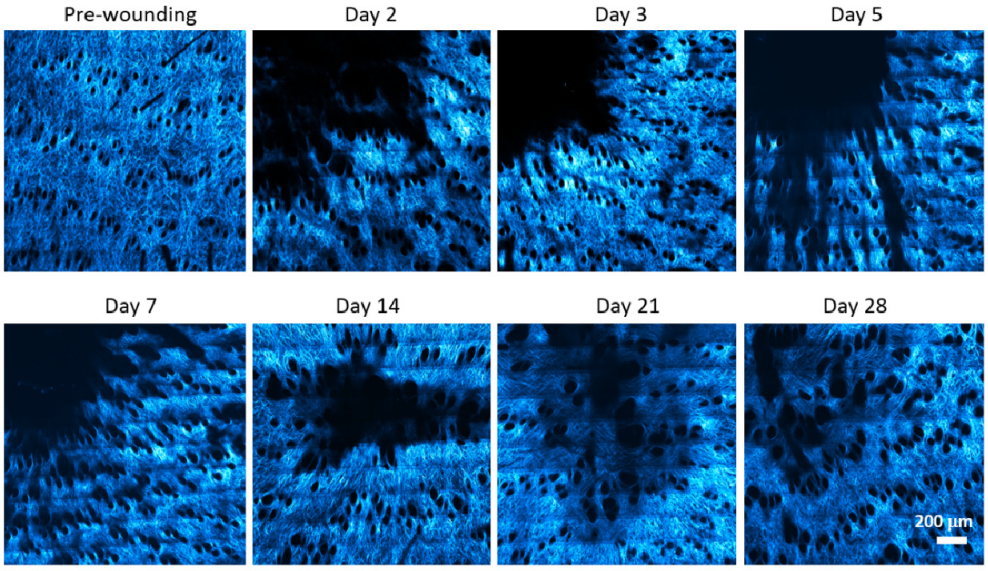

Fig. 2. Representative SHG images of the wounded skin from the wounded group with rMuIL-12 injection showing wound healing progression. Scale bar: 200 µm applies to all.

To evaluate the change in collagen structure during the process of wound healing, five small areas around the wound bed on each SHG image of each animal were manually selected, and an ellipse-fit was performed on the magnitude of the 2D Fourier transform of each small image area as described in Section 2.5 [16]. The eccentricity value of the ellipse was used to evaluate the preferred orientation of the collagen fibers immediately around the wound bed, which can be an implication of collagen contraction since the collagen fibers are stretched toward the center of the wound during the contraction process to achieve wound closure [5, 7]. A value closer to 0 suggested that the collagen fibers around the wound were isotropically distributed, and were more similar to the "basket-weave" structure of a non-wounded skin (Fig. 3) [3, 6, 17]. A value closer to 1 suggested that the collagen fibers were oriented in a particular direction (Fig. 3).

#243477 Received 22 Jun 2015; revised 20 Sep 2015; accepted 29 Sep 2015; published 6 Oct 2015

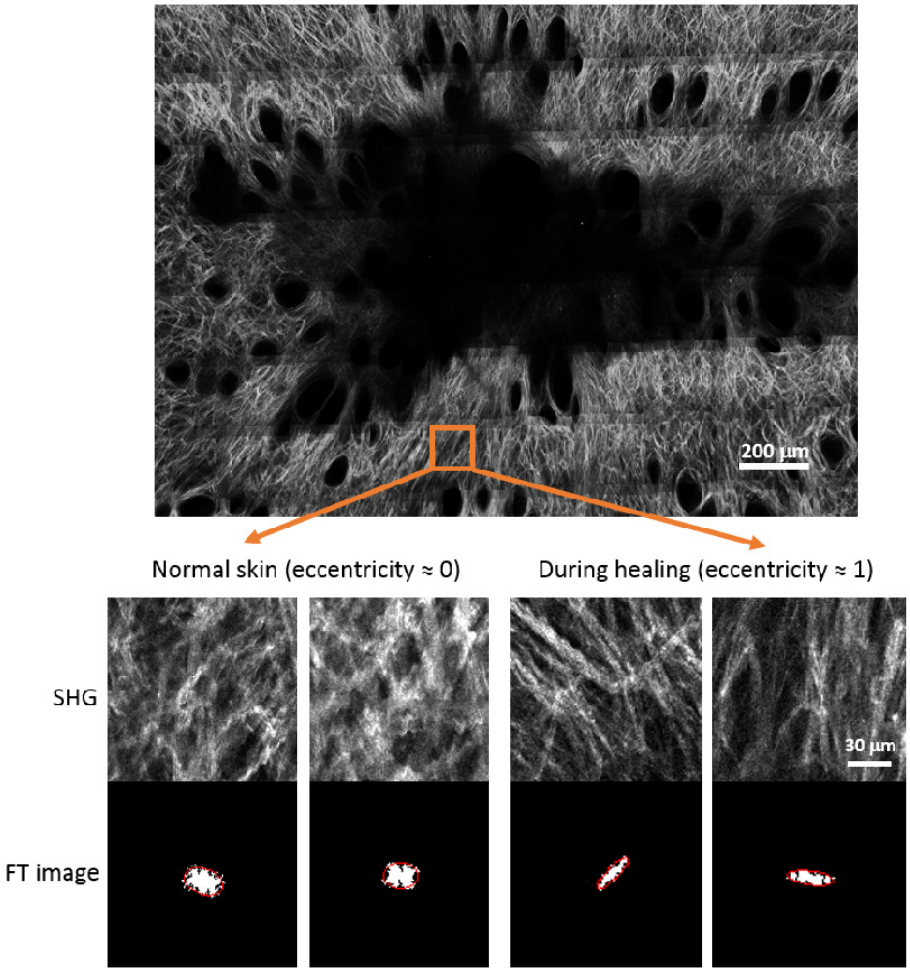

Fig. 3. Analysis of collagen alignment using SHG images. An eccentricity value closer to 0 suggests normal collagen structure, and a value closer to 1 suggests collagen fibers with a preferred orientation. Boxed area in the upper image is a representative example illustrating the size of the small SHG images below. FT stands for Fourier transform.

The alignment analysis was performed on all animals in all three groups, as shown in Fig. 4(a). In the non-wounded with rMuIL-12 group, no noticeable collagen contraction was observed except on day 1, which was most likely caused by hair removal (Fig. 4(b)). Both of the wounded groups showed changes in collagen alignment during the healing process with peaks around day 14, which can be seen in both the Fourier transform of the SHG images (Fig. 4(a)) and the longitudinal tracking of collagen alignment (Fig. 4(b)). One-way ANOVA combined with Tukey HSD test revealed that both of the wounded groups showed a significant increase ($p < 0.05$) in collagen alignment on day 14 compared to the non-wounded group (Fig. 4(b)). This result could suggest that both of the wounded groups showed a significant increase in collagen contraction on day 14, which would be understandable since collagen contraction often follows collagen synthesis and accounts for up to a 40% decrease in wound size [5, 7]. In addition, both of the wounded groups exhibited large variations in the level of collagen alignment since differences in wound healing rates are expected among different animals. Also, the collagen fibers around the wound can experience different levels of collagen contraction, which can be observed in Fig. 2. Furthermore, volumetric SHG data

#243477 Received 22 Jun 2015; revised 20 Sep 2015; accepted 29 Sep 2015; published 6 Oct 2015

throughout a depth of approximately 80 μm of the wounded skin was also acquired to investigate potential changes in collagen structures across different depths. The results showed that there was no observable changes in the collagen alignment within this depth of the dermal layer. Although there could be potential changes in the collagen structure at deeper layers of the dermis, such phenomenon cannot be investigated due to the limit of penetration depth and the loss of SHG signals with increasing depth.

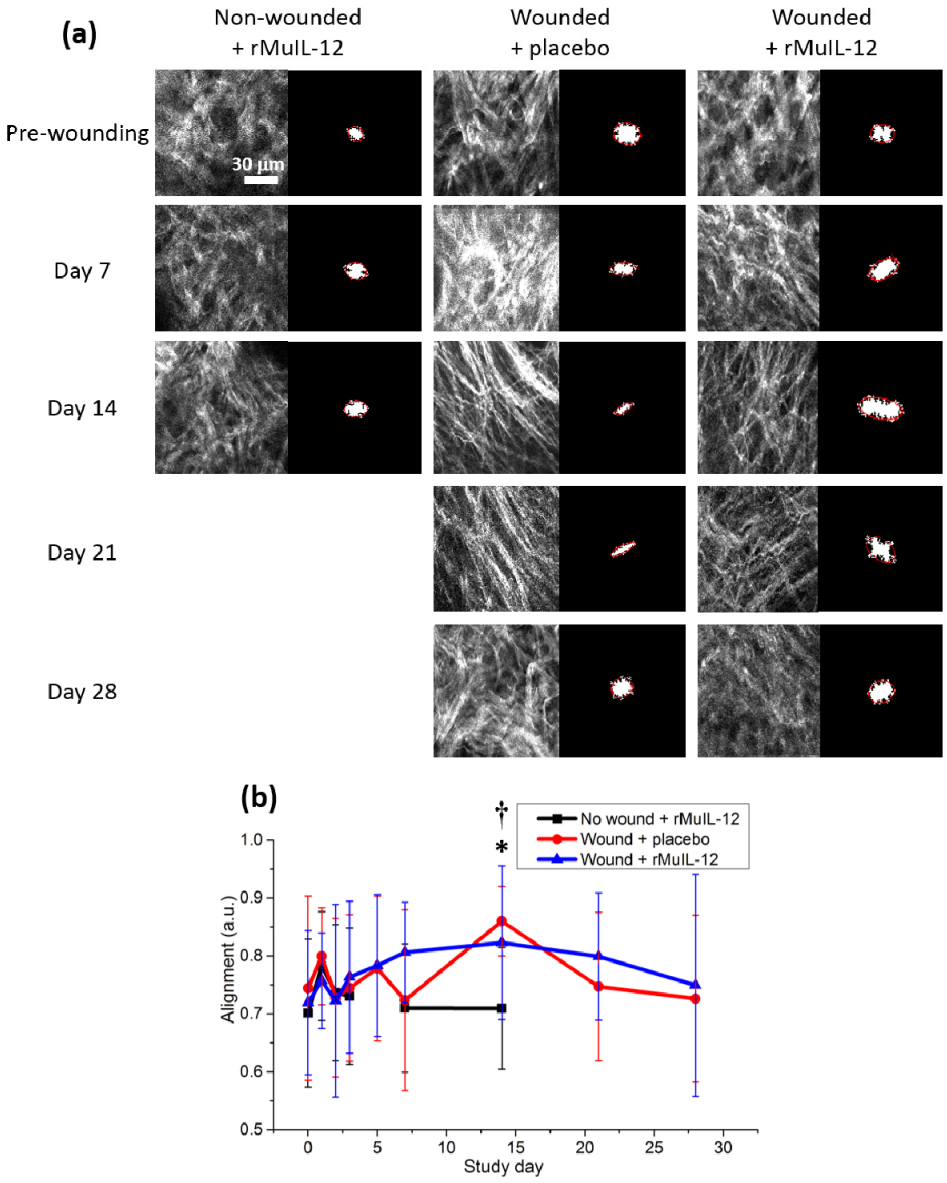

Fig. 4. 2D Fourier transforms show the change in collagen alignment during wound healing. (a) Representative SHG and 2D spatial Fourier transform images from each experimental group on selected imaging days. (b) Longitudinal tracking of collagen alignment/orientation during the one month study period. † Both wounded groups show significantly higher alignment compared to the non-wounded group on day 14 ($p < 0.05$); * in the wounded group with placebo injection, the level of collagen alignment is significantly higher on day 14 compared to days 2, 7, and 28 ($p < 0.05$). Scale bar: 30 μm applies to all.

#243477 Received 22 Jun 2015; revised 20 Sep 2015; accepted 29 Sep 2015; published 6 Oct 2015

Looking at the dynamic trend of collagen alignment in each experimental group, it was found that the level of collagen alignment on day 14 was significantly higher compared to days 2, 7, and 28 in the wounded group with placebo injection ($p < 0.05$, Fig. 4(b)). However, similar differences were not observed in the wounded group with rMuIL-12 injection. While these results may imply that there was a more drastic change in collagen organization in the placebo group during healing, additional studies are necessary to make further conclusions. IL-12 is known to induce the production of IFN-γ, which is one of the effectors of matrix synthesis regulation [1, 3]. In addition, the release of IFN-γ interacts with macrophages, whose main functions include matrix synthesis [3]. Therefore, injection of rMuIL-12 in the wounded mice at the early time point of wound healing can potentially have an effect on the progression of healing. Although additional conclusions cannot be made based on current observations, our results show the heterogeneity of the microenvironment of the wounded skin, and the unique capability of SHG for evaluating the process of collagen regeneration and reorganization. In future studies, additional SHG parameters, such as the polarization of the collagen fibers, should also be characterized to further understand the relationship between IL-12 and the process of matrix synthesis.

3.2 Effect of rMuIL-12 on the metabolic activity in wounded skin

FLIM generates image contrast between different excited-state lifetimes characterized by various fluorescence decay rates of the endogenous fluorophores in tissue [18], and it was used in the study to examine the effect of rMuIL-12 on the metabolic activities in the skin around the wound bed during healing. Figure 5(a) shows representative FLIM images from each experimental group on days 0 (pre-wounding), 2 (24 hours post injection), 3 (48 hours post injection), and 14.

The imaging plane was focused on keratinocytes approximately 2-6 μm deep below the stratum corneum layer in the epidermis, where NADH is the dominant fluorophores and changes in metabolic activity in the skin can be evaluated based on the change in the fluorescence lifetime [11, 19, 20]. Results demonstrated that no significant change in fluorescence lifetime was observed in the non-wounded group. In both of the wounded groups, elevation in the fluorescence lifetime was seen after wounding and injection (blue-shift in Fig. 5(a)), however, only the wounded group that received the rMuIL-12 injection showed a significant increase ($p < 0.05$) in fluorescence lifetime 24 and 48 hours post injection (days 2 and 3), compared to pre-wounding on day 0 (Fig. 5(b)). Statistical analysis also showed that the wounded group with rMuIL-12 injection had significantly longer fluorescence lifetime ($p < 0.05$) than the wounded group with placebo injection on day 2, which was 24 hours post wounding and injection. In addition, the wounded group that received the rMuIL-12 injection demonstrated significantly longer fluorescence lifetime ($p < 0.05$) than the non-wounded group at the 48-hour time point after injection (day 3). These observations suggested that only the wounded group that received the rMuIL-12 injection demonstrated a significant increase in metabolic activity during the early time points of wound healing since an increase in fluorescence lifetime suggests an increase in the cellular metabolic activity [9, 21]. In addition, the results of the cross-group comparison suggested that the wounded group with rMuIL-12 injection showed a faster metabolic response toward the wound compared to the other wounded group, and they also suggested that only the wounded group with rMuIL-12 injection had a significantly larger metabolic response compared to the non-wounded group during the early time point of the wound healing.

#243477 Received 22 Jun 2015; revised 20 Sep 2015; accepted 29 Sep 2015; published 6 Oct 2015

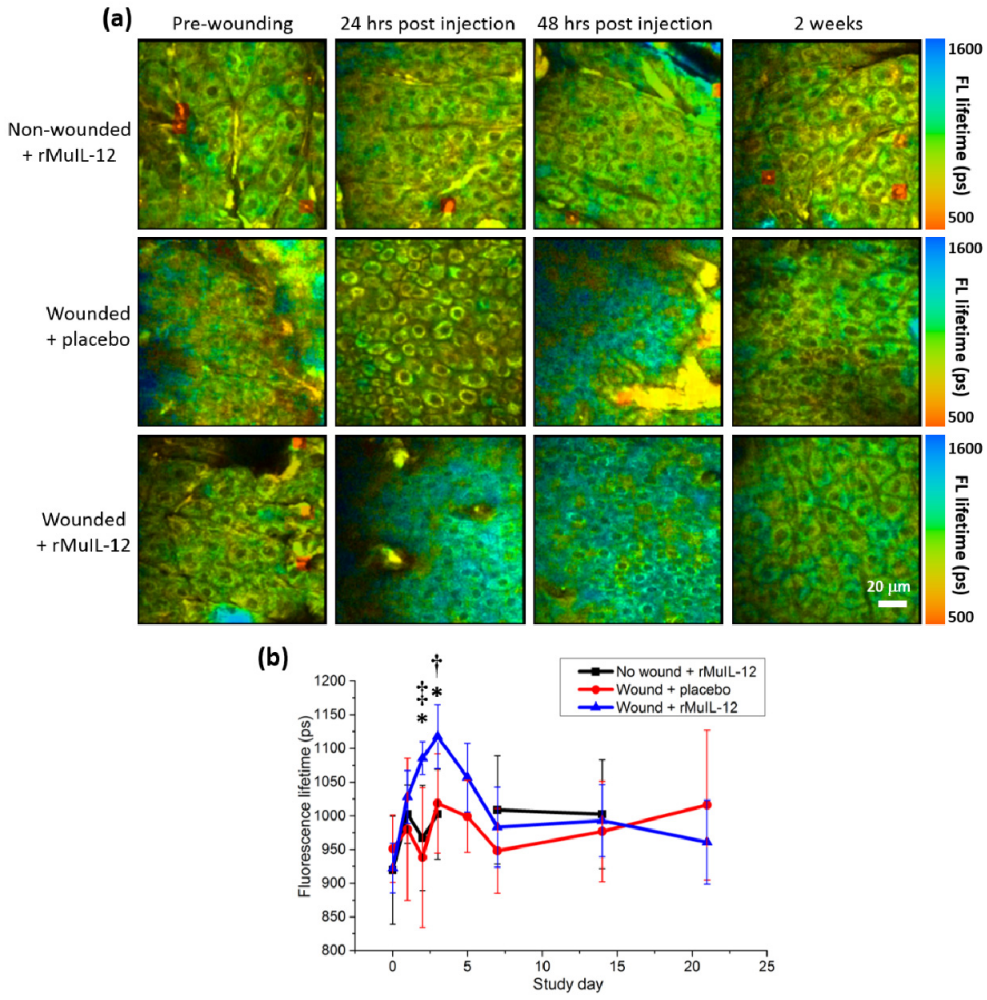

Fig. 5. Dynamics of the metabolic activity in the wounded skin during healing using FLIM. (a) Representative FLIM images from each experimental group on selected days. (b) Longitudinal tracking of the change in fluorescence lifetime during wound healing. ‡ Wounded with rMuIL-12 group has a significantly longer lifetime compared to the wounded with placebo group on day 2 ($p < 0.05$); † wounded group with rMuIL-12 injection has a significantly longer lifetime compared to the non-wounded group on day 3 ($p < 0.05$); * in the wounded with rMuIL-12 group, the lifetimes on days 2 and 3 were significantly longer than day 0 ($p < 0.05$). Scale bar: 20 µm applies to all.

One of the first responses of an organism to pathogens is an inflammatory reaction, which is also an important phase during wound healing that will then lead to tissue repair [1, 7]. During the healing process, there is an increase in energy demand that results in an increase in the metabolic rate in wounded skin [22], which was demonstrated by both of the wounded groups in this study. Longer fluorescence lifetime suggests that there is an increase amount of the protein-bound NADH, which is the long lifetime component of NADH [9, 13]. The protein-bound NADH is associated with oxidative phosphorylation [23], the oxygen-mediated metabolic pathway that is more efficient in energy production in the biological system [24, 25]. The significant increase in fluorescence lifetime we observed in the wounded group that received the rMuIL-12 suggested that the additional IL-12 administration post wounding initiated a significant increase in metabolic rate through the process of oxidative

#243477 Received 22 Jun 2015; revised 20 Sep 2015; accepted 29 Sep 2015; published 6 Oct 2015

phosphorylation to satisfy the higher demand for energy in the healing skin. Our results suggest that IL-12 triggered a greater and more rapid inflammatory response after wounding, which is potentially associated with the significant increase in the metabolic rate. These phenomena may be beneficial to the overall process of wound healing.

4. Conclusion

We demonstrated *in vivo* longitudinal SHG and FLIM imaging and tracking of wound healing post administration of rMuIL-12. Initial observations showed that IL-12 induced a significantly more rapid onset and higher metabolic activity in the wounded skin during the early time points of wound healing. The results suggest that the additional administration of this pro-inflammatory cytokine initiated a stronger inflammatory response that may be beneficial to the overall progression of skin wound healing, and may very likely play a key role in protecting the biological system against radiation damage. Preliminary SHG results showed signs that could imply that the wounded mice with IL-12 injection showed a less drastic change in collagen structure during healing, but additional studies are needed to verify this observation and to make further conclusions about the effect of IL-12 on matrix synthesis or possible correlations with the significant increase in metabolic activity. While additional investigations are required, including the dynamic profiles of the immune cells and changes in wound healing progression in radiation-damaged skin, this MPM imaging technology can offer quantitative, non-invasive longitudinal tracking of cell and tissue dynamics at the cellular-level resolution, so that we can better comprehend the complex mode of action of IL-12.

Acknowledgments

This research was supported by a sponsored research agreement from Neumedicines Inc. We thank Darold Spillman for assistance with logistical and information technology support, and the researchers at Neumedicines for their expert assistance on compound formulation, technical support, and consultation. J.L. was funded by the NIH National Cancer Institute Alliance for Nanotechnology in Cancer (Midwest Cancer Nanotechnology Training Center; R25 CA154015A), and A.J.B. was supported by the National Science Foundation Graduate Research Fellowship (DGE-1144245). This project was entirely funded with federal funds from BARDA/ASPR/DHHS (HHSO100201100037C).

#243477 Received 22 Jun 2015; revised 20 Sep 2015; accepted 29 Sep 2015; published 6 Oct 2015